2011-01-01

A Reduced Order Parameter Estimation Technique Using Orthonormal Wavelets

Miguel Hernandez Iv
University of Texas at El Paso, miguelher@utep.edu

A REDUCED ORDER PARAMETER ESTIMATION TECHNIQUE USING ORTHONORMAL WAVELETS

MIGUEL HERNANDEZ IV

Program in Computational Science

APPROVED:

_____

Leticia Velazquez, Ph.D., Chair

_____

Miguel Argaez, Ph.D., Co-Chair

_____

Christopher E. Kees, Ph.D.

_____

Benjamin Flores, Ph.D.

Acting Dean of the Graduate School

Dedicated with love to

Erika and Miguel V.

A REDUCED ORDER PARAMETER ESTIMATION TECHNIQUE USING ORTHONORMAL WAVELETS

by

MIGUEL HERNANDEZ IV, M.S.E.E., B.S.E.E.

THESIS

Presented to the Faculty of the Graduate School of

The University of Texas at El Paso

in Partial Fulfillment

of the Requirements

for the Degree of

MASTER OF SCIENCE

Program in Computational Science

THE UNIVERSITY OF TEXAS AT EL PASO

December 2011

Acknowledgments

Many people have participated both directly and indirectly to this thesis. Here, I acknowledge your contributions. Beginning with my advisor Leticia Velazquez, thank you for making me a part of your research team. I don't think either of us knew that a simple email asking if I knew how to program in a Linux environment would develop into research in reduced order models with wavelets. I thank you for your understanding, support, and probing questions. Without your faith in my abilities, this thesis would not be possible.

To Miguel Argaez, thank you for introducing me to the world of numerical optimization. That single class has influenced me more than any other. Your ability to break down a complex problem into its fundamental components and the patience you have while explaining each component are inspiring. I also thank you for welcoming me into your research team.

To Christopher Kees, thank you for providing Proteus and for all your help with the installation process. Most of all, thank you for accepting the invitation to sit on my thesis committee.

To my son Miguel V, I am forever grateful for all the times you lifted my spirits and made me laugh. The joy you have brought into my life has been a constant source of motivation, inspiration and energy.

To my beautiful wife Erika, I owe you my deepest gratitude. Thank you for your love, continued encouragement and support. Without you, all my endeavors would be all for naught. I have always and continue to love you a "million trillion".

Erika and Miguel V, this thesis is dedicated to you with all my heart.

Abstract

In this work we introduce methods for model order reduction using orthonormal wavelets. Specifically, we propose techniques and algorithms for wavelet-based reduced order parameter estimation using orthonormal wavelets for solving nonlinear least squares problems. Approaches for parameter reduction using the one dimensional and two dimensional wavelet transforms are presented using multiple levels of decomposition.

The performance of wavelet-based reduced order parameter estimation is tested using a suite of orthonormal wavelets on a groundwater hydraulics model provided by the U.S. Army Corps of Engineers. Using the hydraulics model, the goal is to find a least-squares solution of the permeability field given the pressure field observations such that the discrepancy between the model and the observed behavior of the system is minimized.

The results show that in terms of the number of iterations, time, and error, there exist reduced order parameter estimation models obtained with orthonormal wavelets that can be used in lieu of the full order model. By incorporating these wavelet-based reduced order parameter estimation techniques into nonlinear least squares parameter estimation problems, a faster characterization can be achieved.

Table of Contents

List of Figures

List of Tables

Chapter 1

Introduction

1.1 Motivation

Inverse, least squares and parameter estimation problems have received much attention in diverse fields of science and engineering. Medical imaging [15, 14], geophysics [19], heat transfer [3], quantum, wave, and electromagnetic scattering [26], and electrical impedance tomography [10] are a few examples. In all of these fields, it has been shown that reliable parameter estimation is a cornerstone for improving predictions and reducing the risk of application decisions.

However, as the size of the problem and the number of parameters to estimate increases, the computational cost involved in obtaining a solution also increases. Realistic models are highly complex and can have thousands, millions, and in some cases billions of equations and unknowns that need to be satisfied. Simplification of the model and the underlying parameters is thus needed in order to perform simulations within an acceptable amount of time and to cope with limited memory and storage capacity among other requirements.

To reduce the computational cost of the so-called full order model, model reduction methods have been developed that approximate the full order model and simplify computations by reducing the dimensions of the system in question [11, 18, 5, 2]. Accomplished primarily through singular value decomposition (SVD) based techniques, model reduction is applied to either the forward model, known as model order reduction (MOR), or to the parameters, known as reduced order parameter estimation (ROPE), using what has been termed a "data compression" step in [5]. These SVD model reduction techniques borrow heavily from ideas traditionally found in the area of image processing and transform coding where a subset of singular values are used to approximate and compress an image, i.e. the full order model.

Although model reduction borrows techniques typically found in image processing, it is very surprising that model reduction using wavelets has not received much attention and has not been adequately addressed in the literature. The use of the wavelet transform in image processing is by far the most popular and practical technique used in many applications including JPEG 2000, digital cameras, high definition video, and medical imaging among others. This observation begs the question: Can wavelets be used for model reduction?

1.2 Thesis Contributions and Outline

To this end, in this work we study, explore, and propose methods for model reduction using wavelets. Specifically, we introduce techniques and algorithms for wavelet-based reduced order parameter estimation using orthonormal wavelets for solving nonlinear least squares parameter estimation problems. Approaches for parameter reduction using the one dimensional and two dimensional wavelet transforms are presented using multiple levels of decomposition. The performance of the wavelet-based ROPE is tested using a suite of orthonormal wavelets on a groundwater hydraulics model provided by the U.S. Army Corps of Engineers. With this in mind, this thesis is organized as follows:

Chapter 2: In this chapter, we introduce the nonlinear least squares problem. We then discuss the Simultaneous Perturbation Stochastic Approximation (SPSA) optimization algorithm for solving the nonlinear least squares problem.

Chapter 3: The discrete orthonormal wavelet transform is introduced. The use of the wavelet transform for reduced order parameter estimation is motivated through a discussion and example of data compression and transform coding. The mathematics behind the 1D and 2D wavelet transforms is then introduced. A filter bank approach to the wavelet transform with multilevel decomposition is presented, and parameter reduction using 1D and 2D wavelets is discussed.

Chapter 4: Methods for solving the nonlinear least squares optimization problem using a modified SPSA algorithm are proposed that use one dimensional and two dimensional wavelet-based reduced order parameter estimation. Then, the Proteus Computational Methods and Simulation

Toolkit is introduced. Using Proteus, an inverse problem is formulated to evaluate the performance of wavelet-based reduced-order parameter estimation. The performance using a suite of 22 orthonormal wavelets at 3 levels of decomposition is then compared.

Chapter 5: In this chapter, a summary of the results is provided and future research ideas and directions are mentioned.

Chapter 2

Nonlinear Least Squares

In this chapter, we introduce the nonlinear least squares problem. We then discuss the Simultaneous Perturbation Stochastic Approximation (SPSA) optimization algorithm for solving the nonlinear least squares problem.

2.1 Mathematical Formulation

Consider a nonlinear system where the relationship between the model parameters (input) x and data observations (output) y take the form

$$M(x) = y \tag{2.1}$$

and $M(x)$ is a nonlinear forward model which may or may not have an analytical expression. If we know x and wish to obtain the result y, Eq. (2.1) is said to be a forward problem; however, if we wish to find the cause which produced a set of effects, then we must solve an inverse problem and estimate the x which generated y. To do so, Eq. (2.1) can be posed as the nonlinear least squares (NLSQ) optimization problem in Eq. (2.2) where we seek the x which minimizes the residual between the model and observations [24].

Now, consider the nonlinear least-squares parameter estimation problem shown in Eq. (2.2).

$$\min_x f(x) = \frac{1}{2} \left\| R(x) \right\|^2 . \tag{2.2}$$

Here, $f : \mathbb{R}^n \to \mathbb{R}$ is the objective function to be minimized, $R : \mathbb{R}^n \to \mathbb{R}^m$ produces a vector of residuals that measures the discrepancy between the model and its corresponding observations,

and $x \in \mathbb{R}^n$ is a vector of unknown model parameters with $m \geq n$ [17]. The objective function $f(x)$ can also be expressed in the following equivalent forms:

$$f(x) = \frac{1}{2} R(x)^T R(x) = \sum_{i=1}^{m} r_i(x)^2 \tag{2.3}$$

where $r_i(x) : \mathbb{R}^n \to \mathbb{R}$ is the i_{th} residual in the residual vector shown in Eq. (2.4).

$$R(x) = \begin{bmatrix} r_1(x) & r_2(x) & \cdots & r_n(x) \end{bmatrix}^T. \tag{2.4}$$

The residual vector can be written explicitly as the difference between the model and the observations in Eq. (2.5)

$$R(x) = M(x) - y \tag{2.5}$$

where $y \in \mathbb{R}^m$ is a vector of data observations and $M : \mathbb{R}^n \to \mathbb{R}^m$ is the nonlinear forward model. Combining Eqs. (2.5) and (2.2) yields the NLSQ parameter estimation problem shown in Eq. (2.6).

$$\min_x f(x) = \frac{1}{2} \|M(x) - y\|^2. \tag{2.6}$$

Solving Eq. (2.6) over a reduced parameter space $\hat{x} \in \mathbb{R}^r$ with $r << n$ is the focus of this thesis.

2.2 Simultaneous Perturbation Stochastic Approximation

To solve the nonlinear least-squares optimization problem in Eq. (2.6), the Simultaneous Perturbation Stochastic Algorithm (SPSA) introduced in [21] is used. SPSA is a stochastic steepest descent method similar to the deterministic steepest descent method which seeks to minimize an objective function $f : \mathbb{R}^n \to \mathbb{R}$ according to the update equation

$$x_{k+1} = x_k - a_k \nabla f_k \tag{2.7}$$

where $x \in \mathbb{R}^n$ and $\nabla f_k \in \mathbb{R}^n$ is a stochastic gradient computed as

$$\nabla f_k = \begin{bmatrix} \frac{f(x_k + c_k\Delta_k) - f(x_k - c_k\Delta_k)}{2c_k\Delta_{k_1}} \\ \vdots \\ \frac{f(x_k + c_k\Delta_k) - f(x_k - c_k\Delta_k)}{2c_k\Delta_{k_n}} \end{bmatrix} = \frac{(f^+ - f^-)}{2c_k} \begin{bmatrix} \frac{1}{\Delta_{k_1}} \\ \vdots \\ \frac{1}{\Delta_{k_n}} \end{bmatrix} \tag{2.8}$$

with

$$f^+ = f(x_k + c_k\Delta_k), \quad f^- = f(x_k - c_k\Delta_k) \tag{2.9}$$

and $\Delta_k \in \mathbb{R}^n$ is a random perturbation vector chosen from an independent and identically distributed (i.i.d) 0 mean probability distribution. While many distributions meet the 0 mean requirement, the one typically selected is Bernoulli with $P(-1) = P(1) = \frac{1}{2}$. The gain control quantities a_k and c_k in Eqs. (2.7) and (2.8) are defined as

$$a_k = \frac{a}{(A + k + 1)^\alpha} \tag{2.10}$$

$$c_k = \frac{c}{(k + 1)^\gamma} \tag{2.11}$$

where a, c, A, α and γ are strictly positive. The choice of a_k and c_k are crucial to the performance of SPSA and guidelines for choosing them are provided in [21].

Observe in Eq. (2.8) that only 2 function evaluations f^+ and f^- are needed to obtain the gradient approximation ∇f_k independent of the dimension n of the parameter space x. It is this property that makes SPSA attractive in situations where the nonlinear forward model $M(x)$ is computationally expensive to evaluate.

The SPSA algorithm is shown in Algorithm 1 and a complete discussion of the SPSA algorithm can be found in [22].

Algorithm 1 Simultaneous Perturbation Stochastic Approximation

Input: $x_0 \in \mathbb{R}^n, \quad a, c, A, \alpha, \gamma > 0$

Output: x^*

1: **for** $k = 0$ **to** $MaxIters - 1$ **or** until convergence **do**

2: Update gain sequences.

$$a_k = a/\left(A + k + 1\right)^{\alpha} \tag{2.12}$$

$$c_k = c/(k+1)^{\gamma} \tag{2.13}$$

3: Generate simultaneous perturbation vector Δ_k from a zero mean i.i.d. distribution, $\Delta_k \in \mathbb{R}^n$

4: Evaluate objective function around x_k.

$$f^+ = f\left(x_k + c_k\Delta_k\right) \tag{2.14}$$

$$f^- = f\left(x_k - c_k\Delta_k\right) \tag{2.15}$$

5: Approximate ∇f_k.

$$\nabla f_k = \frac{(f^+ - f^-)}{2c_k} \begin{bmatrix} \frac{1}{\Delta_{k_1}} \\ \vdots \\ \frac{1}{\Delta_{k_n}} \end{bmatrix} \tag{2.16}$$

6: Update.

$$x_{k+1} = x_k - a_k \nabla f_k \tag{2.17}$$

7: **end for**

8: **return** x^*

Chapter 3

The Discrete Orthonormal Wavelet Transform

In this chapter, the discrete orthonormal wavelet transform is introduced. We begin with a discussion of the energy compaction property of the wavelet transform to motivate its use for parameter reduction. Then, we cover the basic mathematics behind the 1 dimensional and 2 dimensional wavelet transforms using a filter bank approach for multilevel decomposition. Finally, we show how the wavelet transform can be used to reduce the dimension of the parameter space from n to r.

3.1 Data Compression and the Relationship to Reduced Order Parameter Estimation

The motivation for using the wavelet transform to reduce the dimension of the unknown parameters x in Eq. (2.6) comes from the fields of image processing, image compression, and transform coding. In these fields, huge amounts of information (for example, images) are transmitted over limited-bandwidth communication lines and networks such as the Internet. For fast transmission and to reduce storage requirements, these signals must be compressed. In short, the goal of data compression is, given a signal $x \in \mathbb{R}^n$, find a lower dimensional signal $\hat{x} \in \mathbb{R}^r$ with $r < n$ to transmit or store that approximates x. The most widely used techniques for data compression are based on the wavelet transform.

The key to using wavelets to find the lower dimensional signal $\hat{x}$ lies in a property known as energy compaction. It is well known in the literature that the wavelet transform tends to concentrate

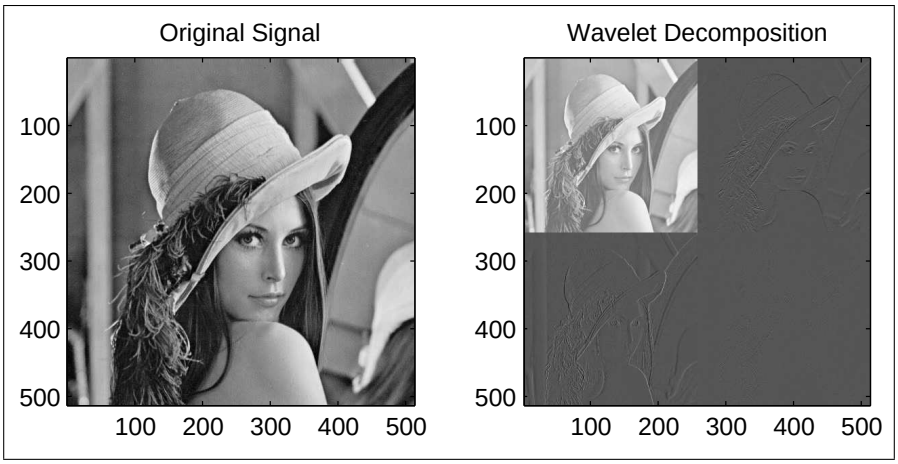

Figure 3.1: Original signal x and the corresponding wavelet decomposition. The upper left subband is the low frequency information and represents the low dimensional approximation to x

energy in the low frequency subband of the wavelet decomposition [1] [27]. Energy is related to the ℓ_2-norm and defined as [20]

$$\varepsilon = \|x\|^2 = \sum_i x_i^2. \tag{3.1}$$

To illustrate the energy compaction property, consider Figure 3.1. Here, we have the original signal $x \in \mathbb{R}^{512\times512}$ and its corresponding wavelet transform decomposition also in $\mathbb{R}^{512\times512}$. Notice that the upper left quadrant of the wavelet decomposition is a low dimensional approximation $\hat{x} \in \mathbb{R}^{256\times256}$ that is one-fourth the size of the original signal and corresponds to the low frequency subband wavelet coefficients. Using Eq. (3.1), we quantify the amount of energy contained in $\hat{x}$ and find that it contains 95.75% of the energy using only one-fourth of the coefficients.

Since $\hat{x}$ contains most of the energy, a simple data compression scheme would be to make all of the other wavelet subbands zero and preserve only the low frequency information as in Figure 3.2. Using only $\hat{x}$, we can reconstruct an approximation of x using the inverse wavelet transform as in Figure 3.3. To the human eye, the difference between the original signal and the approximation may not be readily detected. To measure how well $\hat{x}$ approximates the original signal, the average of the sum of the squared errors is commonly used in image processing. Also known as the mean

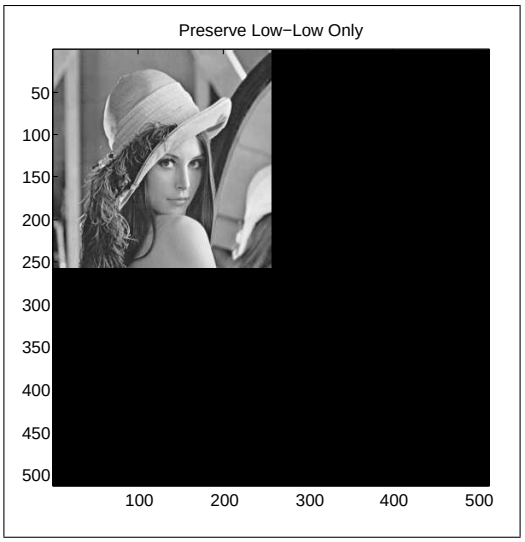

Figure 3.2: From each subband, only preserve the low-low frequency information in $\hat{x}$. Set all other subband coefficients, i.e. the high pass coefficients, to zero.

squared error, it is defined as

$$MSE = \frac{1}{n}\sum_{i=1}^{n}(x_i - y_i)^2 = \frac{1}{n}\|x - y\|^2. \tag{3.2}$$

where x and y are two signals we want to compare. Using this measure, we find that the mean squared error between the original signal and the approximation is 6.82×10^{-4}.

It becomes clear that by exploiting the property of energy compaction, the wavelet transform offers a way to reduce the dimension of the unknown parameter space x in Eq. (2.6). In the next section, the wavelet transform is discussed.

3.2 The Wavelet Transform

To reduce the number of parameters to optimize in Eq. (2.6), the full parameter space x is projected onto a lower-dimensional space using the discrete wavelet transform (DWT) [23]. In this section, the DWT is discussed. For a complete treatment of wavelets and wavelet filter banks, see [6].

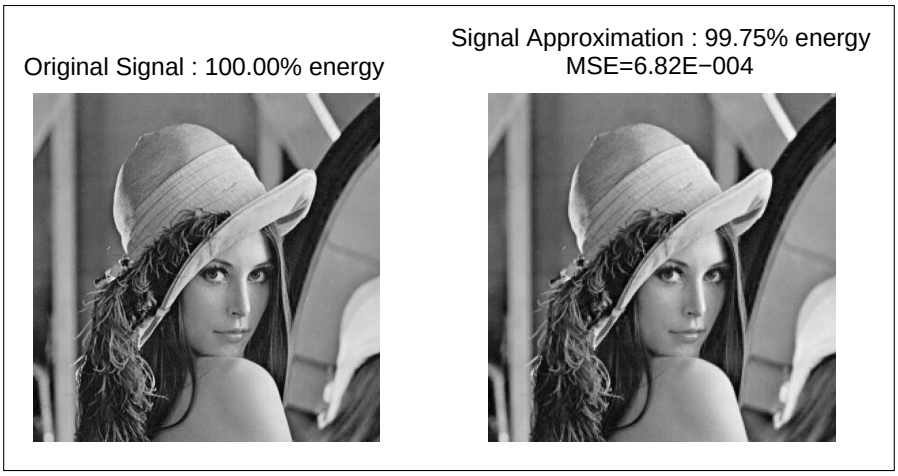

Figure 3.3: A side-by-side comparison of the original signal x and a reconstructed approximation using only the low-low frequency information in $\hat{x}$. $\hat{x}$ contains 99.75% of the energy in x. The mean-squared error is 6.82×10^{-4}

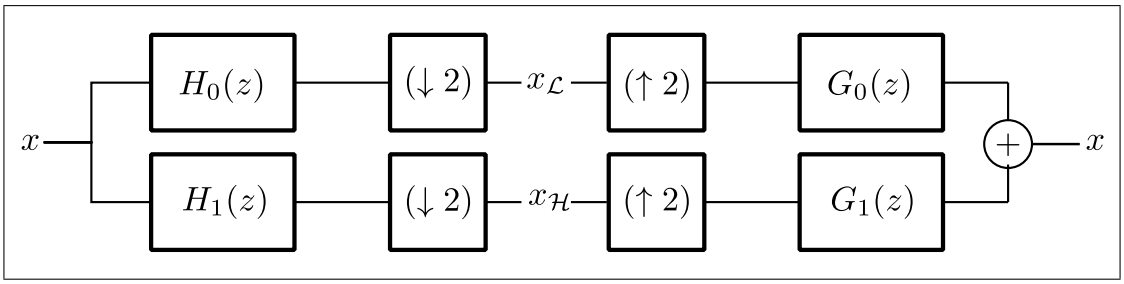

Figure 3.4: 1 Dimensional Wavelet Transform Filter Bank (1 Level of Decomposition)

3.2.1 1D Wavelet Transform

The 1 dimensional (1D) forward DWT is taken by filtering a signal $x \in \mathbb{R}^n$ through a series of filter banks where n is an integer power of 2. The filtering operation involves convolving x through both low pass and high pass filters followed by decimation by a factor of 2 as seen in Figure 3.4 where $H_0(z)$ and $H_1(z)$ are low and high pass wavelet filters in the z-transform domain, $\downarrow 2$ denotes decimation by a factor of 2, and $x_{\mathcal{L}}$ and $x_{\mathcal{H}}$ are the low pass and high pass coefficients that form $\bar{x} \in \mathbb{R}^n$, the signal in the wavelet domain.

The original signal x is reconstructed (or recovered) using the inverse DWT (IDWT). The IDWT is taken by interpolating $x_{\mathcal{L}}$ and $x_{\mathcal{H}}$ by a factor of 2, passing the coefficients through the filters $G_0(z)$ and $G_1(z)$, and then adding the signals together. The convolution operation followed

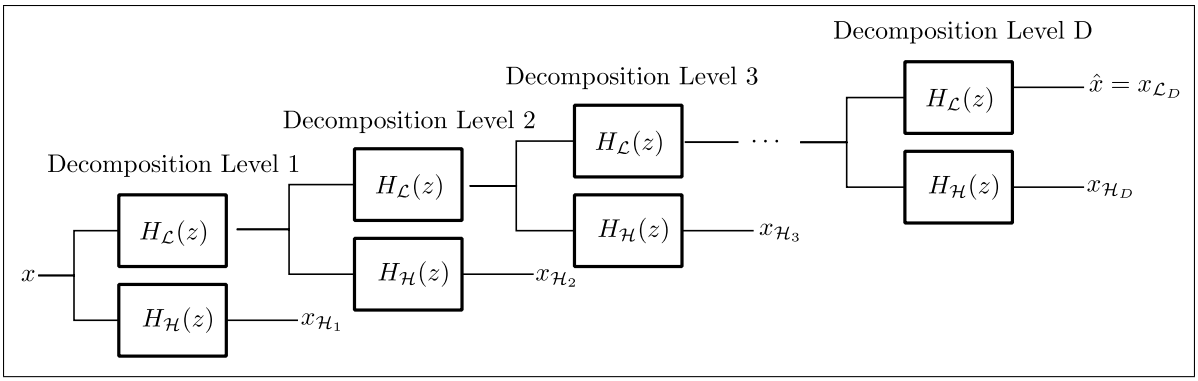

Figure 3.5: 1D Wavelet Transform Filter Bank at Decomposition Level D

by decimation can be expressed as

$$\begin{bmatrix} x_{\mathcal{L}} \\ x_H \end{bmatrix} = \begin{bmatrix} (\downarrow 2)\sum_{\tau} h_0[k-\tau]x[\tau] \\ (\downarrow 2)\sum_{\tau} h_1[k-\tau]x[\tau] \end{bmatrix} = \begin{bmatrix} \sum_{\tau} h_0[k-2\tau]x[\tau] \\ \sum_{\tau} h_1[k-2\tau]x[\tau] \end{bmatrix} \tag{3.3}$$

where k denotes signals and filters in the discrete-time domain.
The coefficients of h_0 satisfy the conditions in Eqs. (3.4) and (3.5) [28].

$$\sum_i h_{0_i} = \sqrt{2} \tag{3.4}$$

$$\sum_i h_{0_i}^2 = 1. \tag{3.5}$$

Eq. (3.5) means that the energy in the wavelet filter is normalized to 1 and will lead to an orthonormal wavelet transform where the energy in the original signal is equal to the energy of the signal in the wavelet domain [16].

When the filter-bank is iterated D times as shown in Figure 3.5, a DWT at decomposition level D is obtained. Here, $H_{\mathcal{L}}$ and $H_{\mathcal{H}}$ are used to simplify the filter bank notation and represent the combination of $H_0(z)$ and $H_1(z)$ with $(\downarrow 2)$ (compare to Figure 3.4). The from this point forward, the DWT at decomposition level D shall be denoted by Eq. (3.6)

$$\bar{x} = \Psi\{x\} \tag{3.6}$$

where $\bar{x} \in \mathbb{R}^n$. $\bar{x}$ shall be defined by taking the output coefficients at each level of decomposition shown in Figure 3.5 and arranging them by decomposition level into a set of subbands as seen in Eq. (3.7)

$$\bar{x} = \left\{ \begin{array}{c} \hat{x} \\ \\ \tilde{x} \end{array} \right\} \tag{3.7}$$

where

$$\hat{x} = x_{\mathcal{L}_D} \tag{3.8}$$

$$\tilde{x} = \left\{ x_{\mathcal{H}_D}, x_{\mathcal{H}_{D-1}}, \cdots, x_{\mathcal{H}_2}, x_{\mathcal{H}_1} \right\}. \tag{3.9}$$

In the signal processing and wavelet community, $\hat{x} \in \mathbb{R}^r$ are called the approximation coefficients at decomposition level D obtained by iterating the filter bank with the low frequency information $x_{\mathcal{L}}$ as the input at each iteration. The remaining coefficients $\tilde{x} \in \mathbb{R}^{n-r}$ are called the detail coefficients. The dimension r of $\hat{x}$ can be determined according to

$$r = \frac{n}{2^D}. \tag{3.10}$$

Eq. (3.10) is obtained using Figure 3.5 and tracing the input x through the filter bank. At the end of each decomposition level, the output has gone through one decimation operator $(\downarrow 2)$ and results in a reduction of length by a factor of 2 at each level. This leads to the following property:

Property 1 *Given $x \in \mathbb{R}^n$ where n is required to be an integer powers of 2, the maximum number of times the filter bank can be iterated, i.e. the maximum decomposition level is $D_{MAX} = \log_2(n)$.*

Proof: The smallest possible value of r is 1. Setting $r = 1$ and solving for D_{MAX} yields

$$\begin{aligned} 1 &= \frac{n}{2^{D_{MAX}}} \\ 2^{D_{MAX}} &= n \\ D_{MAX} &= \log_2(n). \end{aligned} \tag{3.11}$$

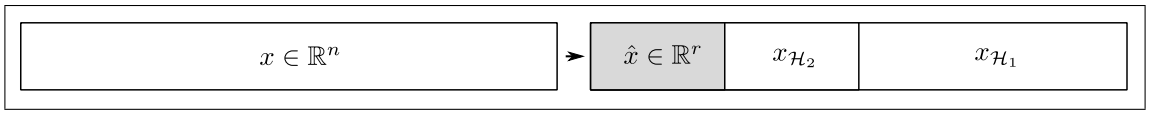

Figure 3.6: Parameter Reduction Using 1D Wavelets. Using the energy compaction property, the parameter space can be reduced from $x \in \mathbb{R}^n$ to $\hat{x} \in \mathbb{R}^r$

.

The dimension of each of the vectors $x_{\mathcal{H}_d} \in \mathbb{R}^{q_d}$ in $\tilde{x}$ from Eq. (3.9) can be determined by

$$q_d = \frac{n}{2^d} \quad d = 1, 2, \ldots, D. \tag{3.12}$$

By iterating the filter bank in Figure 3.5 D times where $D \leq D_{MAX}$ and using the energy compaction property of wavelets as discussed in Chapter 3.1, we can reduce the parameter space of x (see Figure 3.6). Using the 1D wavelet transform on x, the low frequency subband of $\bar{x}$ becomes the reduced parameter space $\hat{x} \in \mathbb{R}^r$. Thus, the wavelet transform can be used to reduce the dimension of the parameter space from n to r.

3.2.2 2D Wavelet Transform

The 2 dimensional (2D) forward DWT is taken by filtering a signal $x \in \mathbb{R}^{n_1 \times n_2}$ through a series of 1D filter banks where n_1 and n_2 are both integer powers of 2. To perform the 2D DWT, the rows of x are filtered and then the columns. When the filter bank is iterated D times, a 2D DWT at decomposition level D is obtained as seen in Figure 3.7.

Denoting the 2D DWT at decomposition level D as

$$\bar{x} = \Psi\{x\} \tag{3.13}$$

and the corresponding wavelet coefficients as $\bar{x}$, $\bar{x}$ shall be defined by taking the output coefficients at each level of decomposition in Figure 3.7 and arranging them by decomposition level into a set

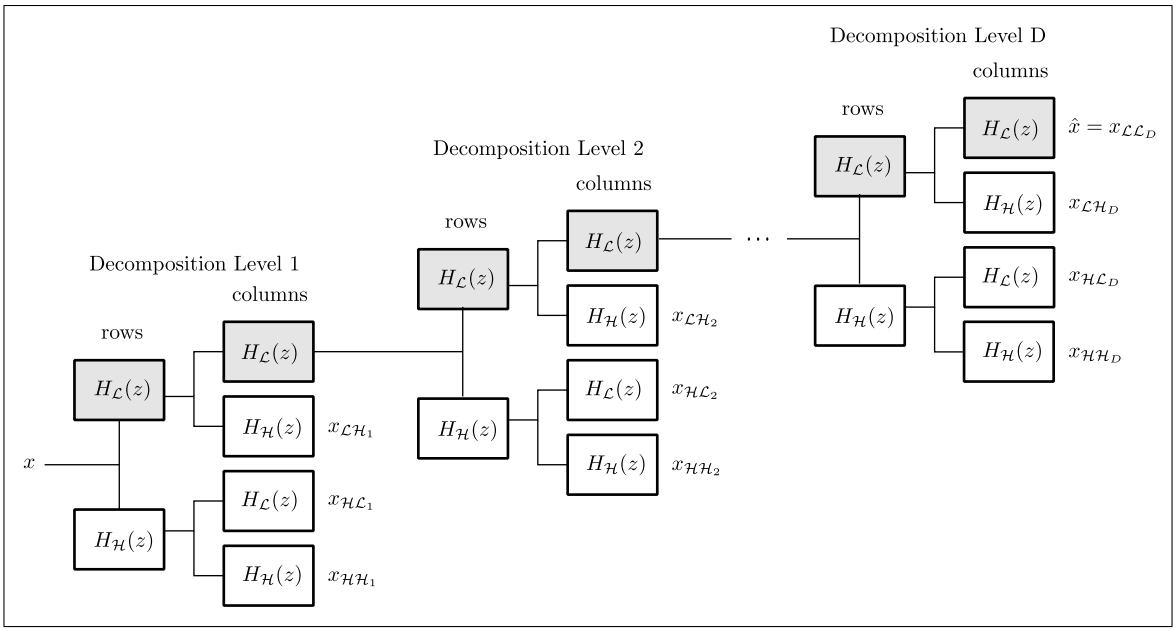

Figure 3.7: 2D Wavelet Transform Filter Bank at Decomposition Level D

of subbands as seen in Eq. (3.7) where

$$\hat{x} = x_{\mathcal{L}\mathcal{L}_D} \tag{3.14}$$

$$\tilde{x} = \left\{x_{\mathcal{L}\mathcal{H}_D}, x_{\mathcal{H}\mathcal{L}_D}, x_{\mathcal{H}\mathcal{H}_D}, \cdots, x_{\mathcal{L}\mathcal{H}_d}, x_{\mathcal{H}\mathcal{L}_d}, x_{\mathcal{H}\mathcal{H}_d}, \cdots x_{\mathcal{L}\mathcal{H}_1}, x_{\mathcal{H}\mathcal{L}_1}, x_{\mathcal{H}\mathcal{H}_1}\right\}. \tag{3.15}$$

$\hat{x} \in \mathbb{R}^{(r_1 \times r_2)}$ are called the approximation coefficients at decomposition level D obtained by iterating the filter bank with the low-low frequency information $x_{\mathcal{L}\mathcal{L}}$ as the input at each iteration. The remaining coefficients $\tilde{x}$ are called the detail coefficients. The dimensions $r_1 \times r_2$ of $\hat{x}$ can be determined according to

$$r_1 = \frac{n_1}{2^D} \tag{3.16}$$

$$r_2 = \frac{n_2}{2^D}. \tag{3.17}$$

Eqs. (3.16) and (3.17) are obtained using Figure 3.7 and tracing the input x through the filter bank. At the end of each decomposition level, the rows have gone through one decimation operator $(\downarrow 2)$

and the columns have also gone through one decimation operator $(\downarrow 2)$, resulting in a reduction of row and column length by a factor of 2 at each level. This leads to the following property:

Property 2 *Given $x \in \mathbb{R}^{n_1 \times n_2}$ where n_1 and n_2 are required to be an integer power of 2, the maximum number of times the filter bank can be iterated, i.e. the maximum decomposition level is $D_{MAX} = MIN\{\log_2(n_1), \log_2(n_2)\}$.*

Proof: The smallest possible value for r_1 and r_2 is 1. Setting $r_1 = 1$ and solving for D_{MAX_1} yields

$$\begin{aligned} 1 &= \frac{n_1}{2^{D_{MAX_1}}} \\ \log_2(2^{D_{MAX_1}}) &= \log_2(n_1) \\ D_{MAX_1} &= \log_2(n_1). \end{aligned} \tag{3.18}$$

Similarly the expression for D_{MAX_2} is

$$D_{MAX_2} = \log_2(n_2). \tag{3.19}$$

For a 2D wavelet transform, the maximum decomposition level is limited by the smallest dimension of x and thus on the smaller of D_{MAX_1} and D_{MAX_2}. Then the maximum decomposition level is given by

$$D_{MAX} = \text{MIN}\{\log_2(n_1), \log_2(n_2)\} \tag{3.20}$$

The dimensions for each of $x_{\mathcal{LH}_d}, x_{\mathcal{HL}_d}, x_{\mathcal{HH}_d} \in \mathbb{R}^{q_1 \times q_2}$ from Eq. (3.15) in $\tilde{x}$ can be determined by

$$q_{1_d} = \frac{n_1}{2^i} \tag{3.21}$$

$$q_{2_d} = \frac{n_2}{2^i} \tag{3.22}$$

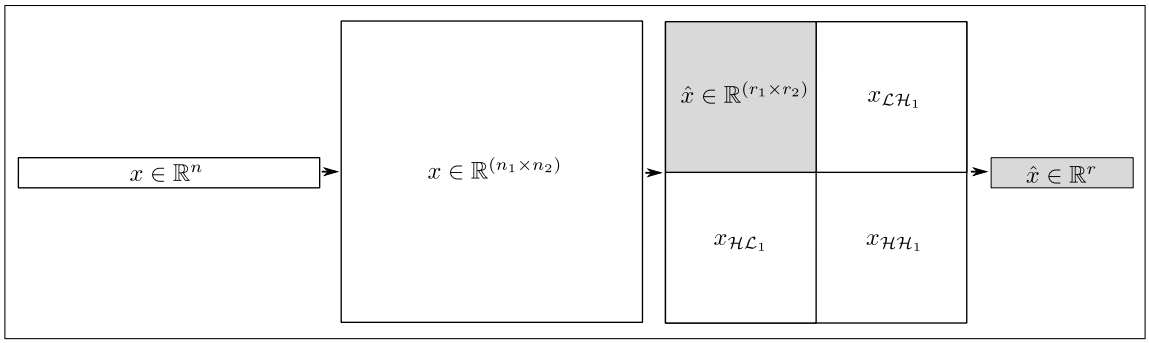

Figure 3.8: Parameter Reduction Using 2D Wavelets. Using the energy compaction property, the parameter space can be reduced from $x \in \mathbb{R}^n$ to $\hat{x} \in \mathbb{R}^r$

with $d = 1, 2, \ldots, D$.

By iterating the filter bank in Figure 3.7 D times where $D \leq D_{MAX}$ and using the energy compaction property as discussed in Chapter 3.1, we can reduce the parameter space of x by reshaping the vector $x \in \mathbb{R}^n$ into a matrix (image) $x \in \mathbb{R}^{(n_1 \times n_2)}$ that satisfies

$$n = n_1 n_2 \tag{3.23}$$

where n_1 and n_2 are integer powers of 2 (see Figure 3.8). Using the 2D wavelet transform at decomposition level D on x, the low frequency subband of $\bar{x}$ becomes the reduced parameter space $\hat{x} \in \mathbb{R}^{(r_1 \times r_2)}$. $\hat{x}$ is then reshaped back into a vector $\hat{x} \in \mathbb{R}^r$ where

$$r = r_1 r_2 \tag{3.24}$$

Thus, the 2D wavelet transform can be used to reduce the dimension of the parameter space from n to r.

Chapter 4

Wavelet-Based Reduced Order Parameter Estimation

In this chapter, we introduce a method for solving the nonlinear least-squares optimization problem using a modified SPSA routine with 1D and 2D wavelet-based reduced order parameter estimation. Then, the Proteus Computational Methods and Simulation Toolkit will be introduced. Using Proteus, an inverse problem is formulated to evaluate the performance of wavelet-based reduced-order parameter estimation. Finally, the performance of wavelet based ROPE using a suite of 22 orthonormal wavelets at 3 levels of decomposition are compared.

4.1 Parameter Reduction Using Wavelets

In Algorithm 2, we propose a routine for solving the NLSQ problem using both 1D and 2D wavelet-based ROPE. Given a 1D or 2D wavelet transform Ψ, the initial estimate x_0 is projected onto a wavelet basis producing a ROPE $\hat{x} \in \mathbb{R}^r$ in step 3. Here, r represents the reduced dimension of $\hat{x}$ at decomposition level D.

After updating the SPSA gain sequences, a simultaneous perturbation vector Δ_k is generated using zero mean i.i.d random variables taken from the Bernoulli distribution $P(-1) = P(2) = \frac{1}{2}$ in step 5.

In step 6, two calculations about $\hat{x}_k$ are obtained in the forward and backward directions. Notice that the detail coefficients $\tilde{x}_k$ are not modified since we are only interested in optimizing over the ROPE $\hat{x}_k$. In this algorithm, we choose to preserve $\tilde{x}_k$ throughout the optimization since the forward wavelet transform provides this extra information "for free"; however, we could set all

Algorithm 2 Wavelet-Based Reduced-Order Modeling

Input: $x_0 \in R^n, \quad a, c, A, \alpha, \gamma > 0$

Output: x^*

1: Given a 1D ($\Psi \equiv \Psi_{1D}$) or 2D wavelet transform ($\Psi \equiv \Psi_{2D}$):

2: **for** $k = 0$ **to** $MaxIters - 1$ **or** until convergence **do**

3: Project x_k onto the wavelet basis. $\hat{x}_k \in \mathbb{R}^r$ represents the reduced order parameter estimate and $\tilde{x}_k$ represents the remaining detail coefficients.

$$\bar{x}_k = \Psi\left\{x_k\right\} = \left\{ \begin{array}{c} \hat{x}_k \\ \tilde{x}_k \end{array} \right\}$$

4: Update SPSA gain sequences. $a_k = a/\left(A + k + 1\right)^{\alpha} \quad c_k = c/(k+1)^{\gamma}$

5: Generate simultaneous perturbation vector $\Delta_k \in R^r$ from a zero mean distribution.

6: Evaluate objective function around $\hat{x}_k$. Make no modifications to $\tilde{x}_k$.

$$\bar{x}^+ = \left\{ \begin{array}{c} \hat{x}_k + c_k\Delta_k \\ \tilde{x}_k \end{array} \right\} \qquad x^+ = \Psi^{-1}\left\{\bar{x}^+\right\} \qquad f^+ = f(x^+) \tag{4.1}$$

$$\bar{x}^- = \left\{ \begin{array}{c} \hat{x}_k - c_k\Delta_k \\ \tilde{x}_k \end{array} \right\} \qquad x^- = \Psi^{-1}\left\{\bar{x}^-\right\} \qquad f^- = f(x^-) \tag{4.2}$$

7: Approximate ∇f_k.

$$\nabla f_k = \frac{(f^+ - f^-)}{2c_k} \left[\begin{array}{c} \frac{1}{\Delta_{k_1}} \\ \vdots \\ \frac{1}{\Delta_{k_r}} \end{array} \right] \tag{4.3}$$

8: Update.

$$\bar{x}_{k+1} = \left\{ \begin{array}{c} \hat{x}_{k+1} \\ \tilde{x}_{k+1} \end{array} \right\} = \left\{ \begin{array}{c} \hat{x}_k - \alpha_k\nabla f_k \\ \tilde{x}_k \end{array} \right\} \tag{4.4}$$

9: Reconstruct x_{k+1}.

$$x_{k+1} = \Psi^{-1}\left\{\bar{x}_{k+1}\right\} \tag{4.5}$$

10: **end for**

11: **return** x^*

coefficients in $\tilde{x}_k = 0$ if we so choose.

Continuing with step 6, once the modified wavelet coefficients in the forward and backward directions $\bar{x}^{\pm}$ are obtained, the full-order parameter space in both directions $x^{\pm}$ are recovered using the inverse wavelet transform. This step is necessary since f (and the nonlinear model $M(x)$ indirectly) expects a vector in $\mathbb{R}^n$ and not in $\mathbb{R}^r$. Using the full order parameter estimates, the forward and backward finite difference approximations are calculated to obtain the gradient approximation in step 7.

In step 8, we update the estimate in preparation for the next iteration; again, the detail coefficients are not modified. Finally, the updated full order parameter estimate is recovered in step 9 and the algorithm is repeated until convergence or the maximum iteration count is exceeded.

The principle difference between the 1D wavelet version and the 2D version for ROPE is that the forward and inverse wavelet transforms operate on a 2D signals (images). With this in mind we introduce the following two procedures $\Psi_{2D}\{x\}$ and $\Psi_{2D}^{-1}\{x\}$ for the 2D forward (Algorithm 3) and inverse (Algorithm 4) wavelet transforms that take care of the necessary vector-to-matrix and matrix-to-vector reshaping.

Algorithm 3 $\Psi_{2D}\{x\}$ (2D Wavelet Transform with Reshaping)

Input: $x \in \mathbb{R}^n$

Output: $\bar{x}$ with $\hat{x} \in \mathbb{R}^r$

1: Reshape the vector $x \in \mathbb{R}^n$ to a matrix $x \in \mathbb{R}^{(n_1 \times n_2)}$ to satisfy Eq. (3.23).

2: Forward 2D wavelet transform

$$\bar{x} = \Psi\{x\} = \left\{ \begin{array}{c} \hat{x} \\ \tilde{x} \end{array} \right\}, \quad \hat{x} \in \mathbb{R}^{(r_1 \times r_2)}. \tag{4.6}$$

3: Reshape $\hat{x} \in \mathbb{R}^{(r_1 \times r_2)}$ to a vector $\hat{x} \in \mathbb{R}^r$ to satisfy Eq. (3.24).

4: **return** $\bar{x} = \left\{ \begin{array}{c} \hat{x} \\ \tilde{x} \end{array} \right\}$

Algorithm 3 takes an input vector $x \in \mathbb{R}^n$ and reshapes it to a matrix $x \in \mathbb{R}^{(n_1 \times n_2)}$ in preparation for the forward 2D wavelet transform in step 1. The forward 2D wavelet transform is taken in step 2 producing $\hat{x} \in \mathbb{R}^{(r_1 \times r_2)}$. To prepare the ROPE for optimization with SPSA, the matrix $\hat{x} \in \mathbb{R}^{(r_1 \times r_2)}$ is reshaped into a vector $\hat{x} \in \mathbb{R}^r$ in step 3. This is necessary since SPSA expects a

vector to optimize over. Finally, the wavelet coefficients in $\bar{x}$ are returned.

Algorithm 4 $\Psi_{2D}^{-1}\{x\}$ (2D Inverse Wavelet Transform with Reshaping)

Input: $\bar{x}$ with $\hat{x} \in \mathbb{R}^r$

Output: $x \in \mathbb{R}^n$

1: Reshape the vector $\hat{x} \in \mathbb{R}^r$ to a matrix $\hat{x} \in \mathbb{R}^{(r_1 \times r_2)}$ to satisfy Eq. (3.24).

2: Inverse 2D wavelet transform

$$\Psi^{-1}\{\bar{x}\} = \Psi^{-1}\left\{ \begin{array}{c} \hat{x} \\ \tilde{x} \end{array} \right\} = x, \quad x \in \mathbb{R}^{(n_1 \times n_2)}. \tag{4.7}$$

3: Reshape $x \in \mathbb{R}^{(n_1 \times n_2)}$ to a vector $x \in \mathbb{R}^n$ to satisfy Eq. (3.23).

4: **return** x

Algorithm 4 is defined to assist with the inverse 2D wavelet transform. The wavelet coefficients in $\bar{x}$ are input into the procedure. The vector $\hat{x} \in \mathbb{R}^r$ is reshaped into a matrix $\hat{x} \in \mathbb{R}^{(r_1 \times r_2)}$ in preparation for the inverse 2D wavelet transform in step 1. The inverse 2D wavelet transform is taken in step 2 producing $x \in \mathbb{R}^{(n_1 \times n_2)}$. The matrix $x \in \mathbb{R}^{(n_1 \times n_2)}$ is reshaped into a vector $x \in \mathbb{R}^n$ in step 3. Finally, x is recovered and returned.

With our wavelet procedures $\Psi_{2D}\{x\}$ and $\Psi_{2D}^{-1}\{x\}$ defined, Algorithm 2 can be used for 2D wavelet-based reduced order parameter estimation to solve the NLSQ problem using a modified SPSA routine. When the 2D wavelet transform is used, the procedures $\Psi_{2D}\{x\}$ (Algorithm 3) and $\Psi_{2D}^{-1}\{x\}$ (Algorithm 4) are used in step 1 of Algorithm 2.

4.2 An Application of Parameter Reduction to Groundwater Hydraulics

In this section, we test the performance of the wavelet-based reduced order parameter estimation technique using both 1D and 2D wavelets on the groundwater hydraulics model provided by the USACE. Since many wavelet transform filters exist, we test the ROPE using a suite of orthonormal wavelets. In addition, we test the scheme using multiple levels of decomposition.

4.2.1 Proteus Computational Methods and Simulation Toolkit

The Proteus computational methods and simulation toolkit (Proteus)[1] is a hydraulics modeling software package developed and maintained by the U.S. Army Corps of Engineers, Engineer Research and Development Center, Coastal and Hydraulics Laboratory [9]. Proteus is a python-based finite element framework designed around the abstract notion of finite elements as a triplet consisting of a geometric element, function space, and a set of unisolvent degrees of freedom [8]. This design allows for the implementation of both multiscale-stabilized conforming Galerkin and discontinuous Galerkin schemes within the same framework and facilitates rapid prototyping of numerical methods. Proteus implements computationally intensive routines in C++, C, and Fortran and is built upon the PETSc toolkit for parallel simulation [4].

The USACE provided a groundwater flow forward model as in Eq. (2.1) where, given the permeability field x and the groundwater flow model in the Proteus model $M(x)$, the corresponding pressure field y is obtained by $M(x) = y$. Figure 4.1 shows the results of the groundwater problem where Figure 4.1a shows the input (true) permeability field and Figure 4.1b shows the output (true) pressure field.

To evaluate the performance of wavelet-based reduced-order modeling, an inverse problem is formulated where the pressure measurement observations y and the hydraulics model $M(x)$ are given and our goal is to find the unknown permeability field x that produced y. Since the hydraulics model cannot be directly inverted, the inverse problem is posed as the nonlinear least-squares optimization problem.

4.2.2 Experimental Setup

In order to evaluate the performance of the wavelet-based ROPE, we formulate a NLSQ problem using the mean-squared error distortion measurement commonly used in image processing from

[1] Proteus was previously known as the Python Adaptive Hydraulics Modeling System (PyADH)

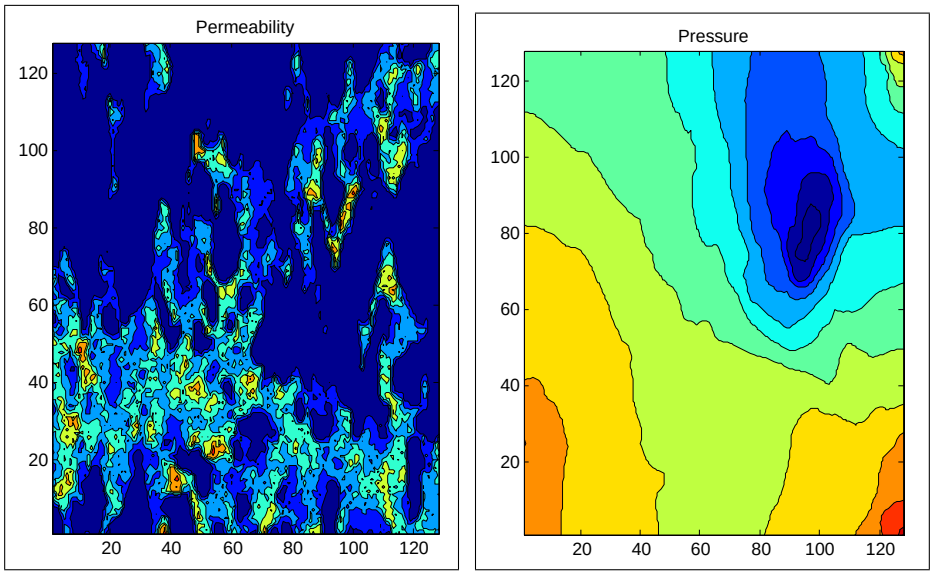

(a) Permeability Field : x (b) Pressure Field : y

Figure 4.1: The permeability and corresponding pressure fields for the groundwater problem, $n = 16384\ (128x128)$

Eq. (3.2). Formally, consider the NLSQ parameter estimation problem shown in Eq. (4.8)

$$\begin{aligned} \min_x f(x) &= \frac{1}{n}\|R(x)\|^2 \\ &= \frac{1}{n}\|M(x) - y\|^2 \\ &= \frac{1}{n}\sum_{i=1}^{n}\left(M_i(x) - y_i\right)^2 \end{aligned} \tag{4.8}$$

where $f : \mathbb{R}^n \to \mathbb{R}$ is the objective function to be minimized, $R(x) \in \mathbb{R}^n$ is a vector of residuals that measures the discrepancy between the Proteus groundwater hydraulics nonlinear model $M : \mathbb{R}^n \to \mathbb{R}^n$ and the corresponding pressure measurements $y \in \mathbb{R}^n$. $x \in \mathbb{R}^n$ is a vector of unknown permeability model parameters which we wish to determine using wavelet-based ROPE. In this problem, $n = 2^{14}$ which corresponds to 16384 permeability unknowns. Figure 4.1 shows the results of the groundwater problem where Figure 4.1b shows the pressure field measurements y and 4.1a shows the true permeability field that we are trying to determine using wavelet-based ROPE.

Table 4.1: Simultaneous Perturbation Stochastic Approximation Optimization Options

SPSA Options	
α	0.602
γ	1.101
a	0.017
c	3.9
A	1000
MaxIterations	500

Table 4.2: Orthonormal Wavelet Options

Orthonormal Wavelet Options	
Haar	haar
Daubechies	db2, db3, db4, db5, db6, db7, db8, db9, db10
Coiflet	coif1, coif2, coif3, coif4, coif5
Symlet	sym2, sym3, sym4, sym5, sym6, sym7, sym8
Decomposition Levels	1 - 3

The SPSA optimization options and parameter values used are displayed in Table 4.1 and are identical to those in [25, 13, 12]. In addition, and since multiple wavelet transforms exist, the wavelet-based ROPE was tested using a suite of orthonormal wavelets from the Haar, Daubechies (db2 - db10), Coiflet (coif1 - coif5), and Symlet (sym2 - sym8) families[2] at decomposition levels 1 - 3 for a total of 66 reduced-order model comparisons as seen in Table 4.2. For each wavelet and decomposition level, the wavelet-based ROPE algorithm was executed until the convergence criteria was met or until the maximum allowed iterations were exceeded. The experiment was executed on both the Ranger high performance computing resource at the Texas Advanced Computing Center and on a Linux workstation. The SPSA and wavelet ROPE algorithms were implemented in C, Octave, Matlab and the WaveLab wavelet library [7].

In order to compare the performance of each of the wavelet-based ROPE schemes, the full order model was executed without wavelet parameter reduction (i.e. SPSA optimization only) to obtain a set of baseline metrics for comparison. Table 4.3 contains the results obtained from the

[2]Wavelet naming conventions used are as defined in MATLAB

Table 4.3: Baseline Metrics Obtained with SPSA Optimization on the Full Order Model

Dim	Wavelet	Lvl	Params	Iters	MSE	FuncCalls	Time (hr)	Final MSE
N/A	N/A	N/A	16384	500	9.22	1500	9.05	9.22

full order model where the metrics are defined as follows:

- Dim - Dimension of the wavelet transform, i.e. 1D or 2D.
- Wavelet - The specific wavelet used for ROPE.
- Lvl - Wavelet decomposition level.
- Params - The number of model parameters to optimize.
- Iters - The number of iterations required to obtain an objective function value less than or equal to the minimum value obtained by SPSA using the full order model.
- MSE - The mean squared error distortion measurement obtained from Eq. (4.8). This measure is also referred to as the "loss value" or simply the error.
- Function Calls - The number of times the objective function was evaluated.
- Time - The amount of time required to obtain an error value less than or equal to the minimum loss value obtained by SPSA using the full order model.
- Final MSE - The final mean squared error value obtained by allowing the algorithm to run to completion.

In the full order model, the minimum MSE obtained by SPSA with no wavelet ROPE was 9.22 at iteration 500, and this value was used as the target/stopping criteria for the wavelet schemes. For comparison purposes, we are interested in the metrics at the point at which the MSE obtained using wavelet-based ROPE is less than or equal to 9.22. Note that in the case of SPSA optimization on the full order model, the "Dim", "Wavelet", and "Lvl" columns contain a value of "N/A" (not applicable) since these values will only apply when ROPE is used.

4.2.3 Results Using 1D Wavelets

Using 1D wavelet-based ROPE, the best performing wavelet at decomposition level 1 was obtained using the 4th order Daubechies wavelet, the best at decomposition level 2 was the 8th order Symlet wavelet, and the best at decomposition level 3 was the 6th order Symlet wavelet. Graphs of the convergence history for each ROPE compared to the convergence of the full order model are shown in Figure 4.2 and the performance metrics are displayed in Table 4.4.

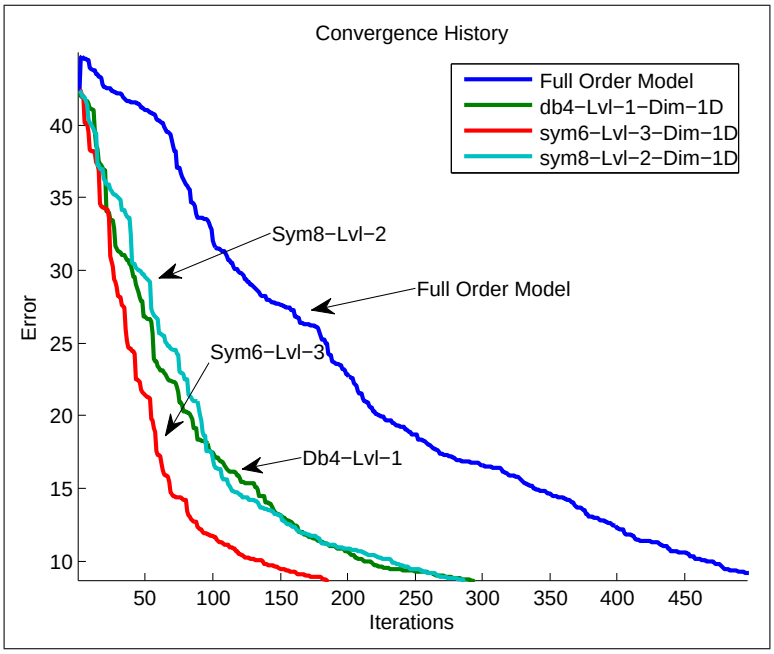

Figure 4.2: The convergence history for 1D ROPE at decomposition levels 1-3 compared to the convergence of the full order model.

Table 4.4: 1D Wavelet-Based Reduced Order Parameter Estimation Comparison

Dim	Wavelet	Lvl	Params	Iters	MSE	FuncCalls	Time (hr)	Final MSE
1D	sym6	3	2048	161	9.19	483	2.91	4.83
1D	sym8	2	4096	262	9.18	786	4.74	5.66
1D	db4	1	8192	261	9.16	783	4.72	5.35
N/A	N/A	N/A	16384	500	9.21	1500	9.05	9.22

From Figure 4.2 and Table 4.4, we see that while all three reduced-order models meet or exceed the target criteria in fewer iterations, the sym6 wavelet ROPE at decomposition level 3 reaches the

target in the fewest iterations. In addition, the sym6 wavelet out performed all other wavelets in each of the defined metrics by optimizing over only 2048 parameters, $1/8$ the size of the full order model. When the algorithm was allowed to run to completion, the sym6 wavelet also produced the smallest MSE value.

Figure 4.3 shows the the permeability, pressure, and convergence history results for the best performing wavelet at decomposition level 3. The graphs contain the following information:

- The top shows the final full order model x_k obtained from $\hat{x}_k$.
- The bottom left shows the final pressure estimate $M(x_k)$ obtained using ROPE.
- The bottom right quadrant shows the convergence history obtained using ROPE compared to the full order model.

See Appendix A and Tables A.1 and A.2 for the results at decomposition levels 1 and 2.

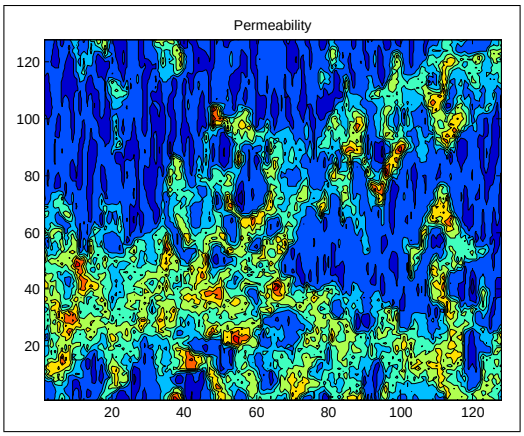

(a) x_k

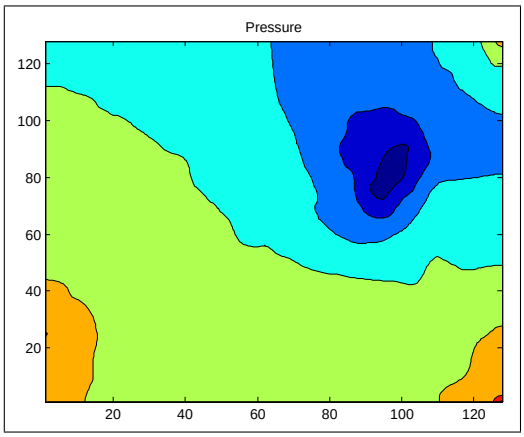

(b) $M(x_k)$

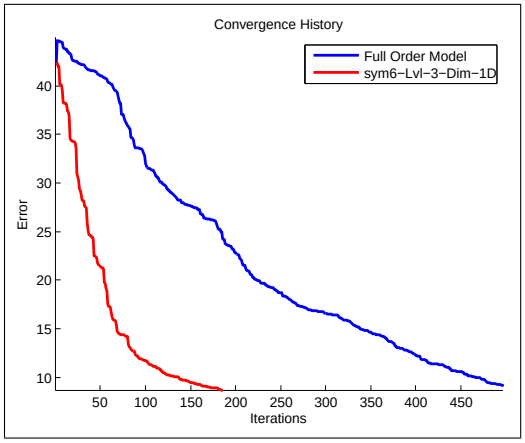

(c) Convergence History Comparison

Figure 4.3: 6th Order Symlet Decomposition Level 3 (1D)

4.2.4 Results Using 2D Wavelets

Using 2D wavelet-based ROPE, the best performing wavelet at decomposition level 1 was obtained using the 5th order Coiflet wavelet, the best at decomposition level 2 was the 8th order Daubechies wavelet, and the best at decomposition level 3 was the 5th order Daubechies wavelet. Graphs of the convergence history for each ROPE compared to the convergence of the full order model are shown in Figure 4.4 and the performance metrics are displayed in Table 4.5.

From Figure 4.4 and Table 4.5, we see that while all three reduced-order models meet or exceed the target criteria in fewer iterations, the db5 wavelet ROPE at decomposition level 3 reaches the

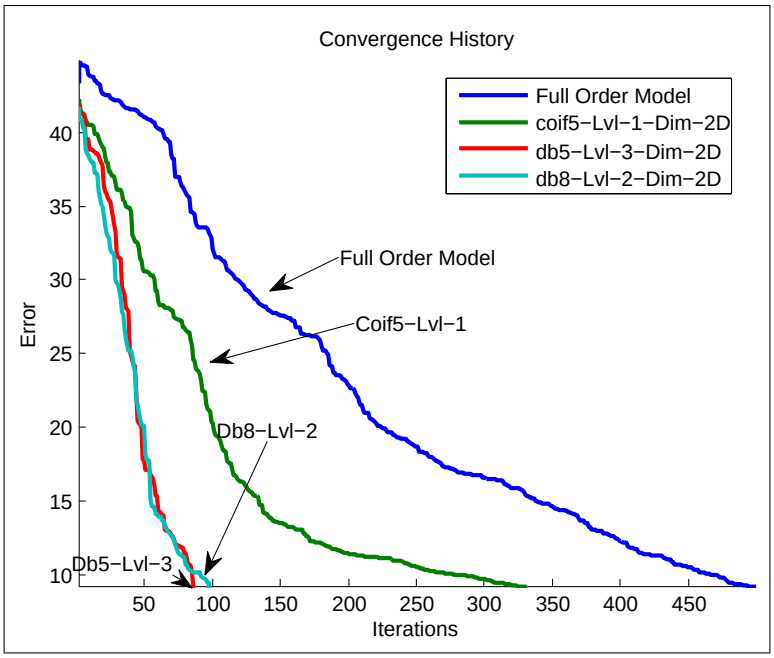

Figure 4.4: The convergence history for 2D ROPE at decomposition levels 1-3 compared to the convergence of the full order model.

Table 4.5: 2D Wavelet-Based Reduced Order Parameter Estimation Comparison

Dim	Wavelet	Lvl	Params	Iters	MSE	FuncCalls	Time (hr)	Final MSE
2D	db5	3	256	85	9.18	255	1.54	3.66
2D	db8	2	1024	97	9.02	291	1.76	3.81
2D	coif5	1	4096	324	9.20	972	5.86	7.04
N/A	N/A	N/A	16384	500	9.21	1500	9.05	9.22

target in the fewest iterations. In addition, the db5 wavelet out performed all other wavelets in each of the defined metrics by optimizing over only 256 parameters, $1/64$ the size of the full order model. When the algorithm was allowed to run to completion, the db5 wavelet also produced the smallest MSE value.

Figure 4.5 shows the the permeability, pressure, and convergence history results for the best performing wavelet at decomposition level 3. The graphs contain the following information:

- The upper left quadrant shows the final ROPE, $\hat{x}_k$.
- The upper right quadrant shows the final full order model x_k obtained from $\hat{x}_k$.

- The lower left quadrant shows the final pressure estimate $M(x_k)$ obtained using ROPE.
- The lower right quadrant shows the convergence history obtained using ROPE compared to the full order model.

See Appendix A and Tables A.3 and A.4 for the results at decomposition levels 1 and 2.

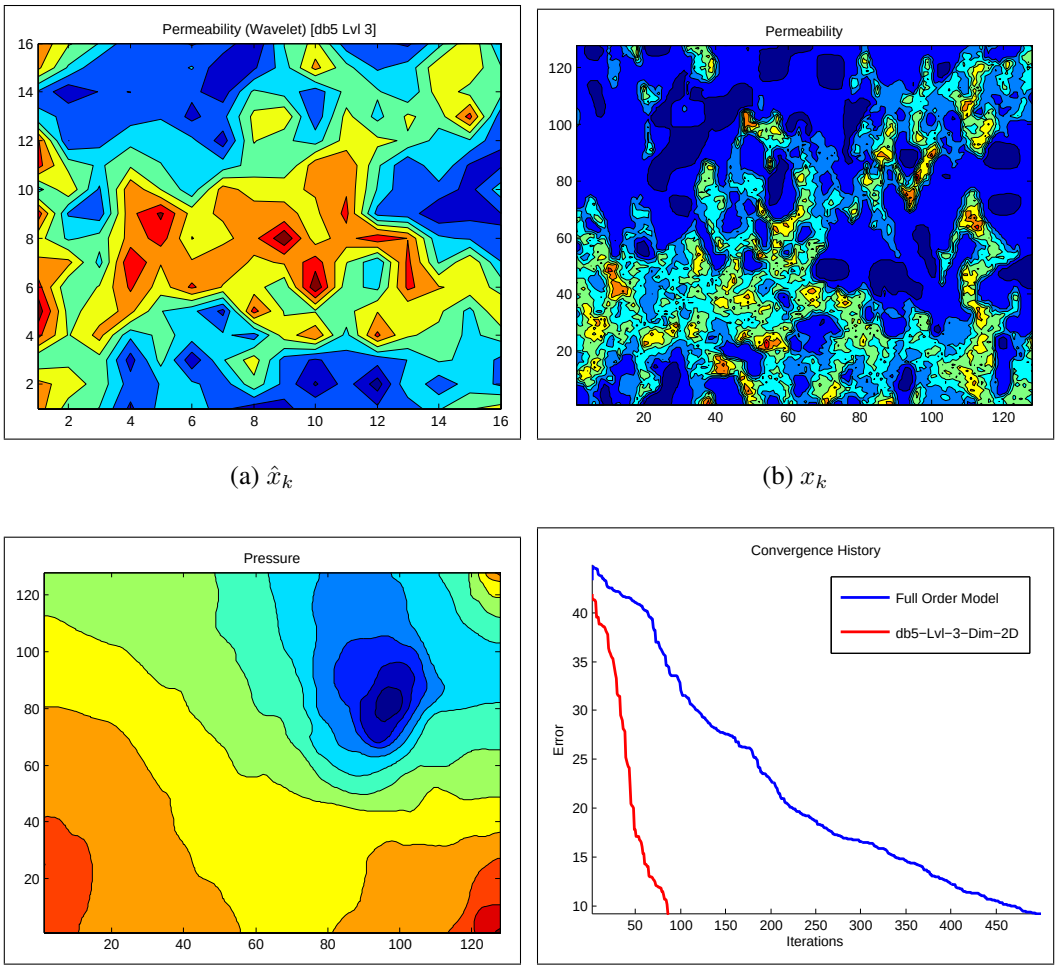

(a) $\hat{x}_k$ (b) x_k

(c) $M(x_k)$ (d) Convergence History Comparison

Figure 4.5: 5th Order Daubechies Decomposition Level 3 (2D)

Chapter 5

Conclusion and Future Research Directions

5.1 Conclusion

In this thesis, we introduced methods for model order reduction using orthonormal wavelets. Specifically, we proposed techniques and algorithms for wavelet-based reduced order parameter estimation using orthonormal wavelets for solving nonlinear least squares problems. Approaches for parameter reduction using the one dimensional and two dimensional wavelet transforms were presented using multiple levels of decomposition.

The performance of wavelet-based reduced order parameter estimation was tested using a suite of orthonormal wavelets on a groundwater hydraulics model provided by the U.S. Army Corps of Engineers. Using the hydraulics model, the goal was to find a least-squares solution of the permeability field given the pressure field observations such that the discrepancy between the model and the observed behavior of the system was minimized.

The results show that in terms of the number of iterations, time, and error, there exist reduced order parameter estimation models obtained with orthonormal wavelets that can be used in lieu of the full order model. By incorporating these wavelet-based ROPE techniques into nonlinear least squares parameter estimation problems, a faster characterization can be achieved.

5.2 Future Research Directions

This research focused on techniques and algorithms for wavelet-based reduced order parameter estimation using orthonormal wavelets for solving nonlinear least squares problems. In this section, we present ideas for future research directions.

First: As stated earlier in this thesis, many orthonormal wavelet transforms exist; however orthonormal wavelets are only one of two classes of wavelet transforms. A class of wavelets exist known as biorthogonal wavelets that can also be used for parameter reduction. The key areas where orthonormal and biorthogonal wavelets differ are:

- The forward and inverse orthonormal wavelet transforms (OWT) satisfy $H^T H = I$; the forward and inverse biorthogonal wavelet transforms (BWT) satisfy $G^T H = I$.
- The OWT preserves the energy of the original signal when projected into the wavelet domain, i.e. $||Hx||^2 = ||x||^2$; the BWT does not preserve energy.
- Biorthogonal wavelets are the only types of wavelets that possess symmetry; orthonormal wavelets cannot possess both orthogonality and symmetry except for the trivial Haar wavelet.

At this point, it is not known if the differences between the OWT and the BWT offer advantages or disadvantages for parameter reduction and requires further study.

Second: From Eq. (3.10), it is clear that the choice of wavelet decomposition level determines the size of the reduced dimension r. In this research, we develop the algorithms for multilevel decomposition, but limit our study to decomposition levels 1,2 and 3 and do not explore the impact of decomposition levels 4, 5, $\cdots$, D_{MAX}. In addition, we do not know a priori what decomposition level will provide the best performance. The optimum choice of decomposition level, and thus the dimension r for wavelet-based parameter reduction remains an open question.

Third: It was stated earlier that model reduction using wavelets has not received much attention and has not been adequately addressed in the literature. In this research, we focused on reducing the number of parameters for the inverse problem using wavelets, but have not considered an application of wavelets to the forward problem to reduce the model M. The most popular methods for model order reduction (MOR) applied to the forward problem include the singular value decomposition (SVD) and Krylov subspace methods. In terms of stability and computational cost, Table 5.1 compares the two methods. MOR using the SVD offers stable results, but can be computationally expensive as the size of the system increases. Krylov subspace methods are inexpensive computationally, but suffer from instability due to error propagations. We postulate that wavelet based

Table 5.1: Model Order Reduction Comparison

Method	SVD	Krylov
Computational Cost	Expensive	Inexpensive
Stability	Stable, Robust	Suffers from Instability

model reduction applied to the forward model lies somewhere in between the SVD and Krylov subspace methods and may offer a balance between computational efficiency while enjoying stability. A study of wavelet-based model order reduction applied to the forward model is necessary, and a comparison of all three techniques must be made to answer this question.

Fourth: Although the results obtained show that we can obtain a reduction in the time required to solve the NLSQ problem and obtain parameter estimates, further improvements in time can still be made. An implementation of wavelet-based ROPE using high performance computing (HPC) techniques will further improve computational time. Examples of HPC implementations include a distributed message passing version using MPI and/or a shared memory version using graphics processing units (GPUs).

Fifth: Apply wavelet based model reduction to other applications. Specifically, the University of Texas at El Paso has a research collaboration with Stanford University and the Department of Defense in which model reduction has been proposed for use in an Underbody Blast study. We propose to apply wavelet based model reduction methods to solve this problem.

References

[1] B.K Al-Abudi and L.A. George. Color image compression using wavelet transform. *International Congress for Global Science and Technology International Journal on Graphics, Vision and Image Processing*, December 2005.

[2] D. Amsallem. *Interpolation on Manifolds of CFG-Based Fluid and Finite Element-Based Structural Reduced-Order Models for On-Line Aeroelastic Predictions(Dissertation)*. Stanford University, 2010.

[3] B.V. Babu and K.K.N Sastry. Estimation of heat transfer parameters in a trickle-bed reactor using dierential evolution and orthogonal collocation. *Computers and Chemical Engineering*, 23, January 1999.

[4] S. Balay, W. D. Gropp, L. C. McInnes, and B. F. Smith. Efficient management of parallelism in object-oriented numerical software libraries, 1997.

[5] K. Carlberg, C. Bou-Mosleh, and C. Farhat. Efficient nonlinear model reduction via a least-squares petrov-galerkin projection and compressive tensor approximations. *International Journal For Numerical Methods in Engineering*, 2009.

[6] I. Daubechies. Ten lectures on wavelets. *SIAM: Society for Industrial and Applied Mathematics*, 1992.

[7] D. Donoho, A. Maleki, and M. Shahram et. al. Wavelab 850.

[8] A. Ern and J.L Guermond. *Theory and Practice of Finite Elements*. Springer-Verlag, 2004.

[9] M.W. Farthing and C.E. Kees. Evaluating finite element methods for the level set equation. Technical Report ERDC/CHL TR-09-11, US Army Corps of Engineers, Engineer Research and Development Center, Coastal and Hydraulics Laboratory, July 2009.

[10] A.D. Garnadi and D. Kurn. 2-D numerical reconstruction of electrical impedance tomography using iteratively regularized gauss-newton algorithms with a-posteriori parameter choice rule. *Sixth Asian Control Conference*, July 2006.

[11] E. Gilden. *Model and Controller Reduction of Large-Scale Structures Based on Projection Methods (Dissertation)*. The University of Texas at Austin, 2006.

[12] M. Hernandez IV, C.E. Kees, M. Argaez, and L. Velazquez. On optimizing reduced-order models of groundwater hydraulics using orthonormal wavelets (submitted, under review). *Journal of Computational and Applied Mathematics*, July 2011.

[13] M HernandezIV, L. Velazquez, and M. Argaez. A comparison of wavelet-based schemes for parameter estimation. *Proceedings of the IEEE Computer Society 2010 Department of Defense High Performance Computing Modernization Program Users Group Conference*, June 2010.

[14] C. Hogea, C. Davtzikos, and G. Biros. An image-driven parameter estimation problem for a reaction-diffusion glioma growth model with mass effects. *Journal of Mathematical Biology*, 56, June 2008.

[15] P.M. Meaney, Q. Fang, and T. Rubaek. Log transformation benefits parameter estimation in microwave tomographic imaging. *Medical Physics*, 34, June 2007.

[16] S.K. Mitra. *Digital Signal Processing: A Computer-Based Approach*. McGraw-Hill, 2nd edition, 2001.

[17] J. Nocedal and S.J. Wright. *Numerical Optimization*. Springer, 2nd edition, 2006.

[18] G. Obinata and B.D.O Anderson. *Model and Controller Reduction of Large-Scale Structures Based on Projection Methods (Dissertation)*. Springer, 2001.

[19] D. Russo. Determining soil hydraulic properties by parameter estimation: On the selection of a model for the hydraulic properties. *Water Resource Research*, 24, 1988.

[20] K. Sayood. *Introduction to Data Compression*. Morgan Kaufmann, 2nd edition, 2000.

[21] J.C Spall. Implementation of the simultaneous algorithm for stochastic optimization. *IEEE Transactions on Aerospace and Electronic Systems*, July 1998.

[22] J.C. Spall. *Introduction to Stochastic Search and Optimization: Estimation, Simulation, and Control*. Wiley-Interscience, 2003.

[23] G. Strang and T. Nguyen. Wavelets and filter banks. *Wellesley-Cambridge Press*, 1996.

[24] A. Tarantola. *Inverse Problem Theory and Methods for Model Parameter Estimation*. Society for Industrial and Applied Mathematics, 2005.

[25] L. Velazquez, M. Argaez, C. Quintero, H. Klie, and M.F. Wheeler. Numerical testing of parameterization schemes for solving parameter estimation problems. *Proceedings of the 26th Army Science Conference*, December 2008.

[26] H. Yamada, K. Yamamoto, Y. Yamaguchi, and M. Sengoku. Scattering parameter estimation accuracy of root-music algorithms in electromagnetic wave scattering measurements. *Electronics and Communications in Japan (Part II: Electronics)*, 79, 1996.

[27] W. Yan, Y. Chen, and S. Tai. Compressing discrete cosine transform coefficients by modified set partitioning in hierarchical trees. *Journal of Electronic Imaging*, 14(4), Dec 2005.

[28] S-H. Yang and W-J. Liao. Perfmance analysis of embedded-wavelet coders. *Journal of Optical Engineering*, 44(9), Sept 2005.

Appendix A

Groundwater Hydraulics Results

A.1 1D Permeability, Pressure and Convergence

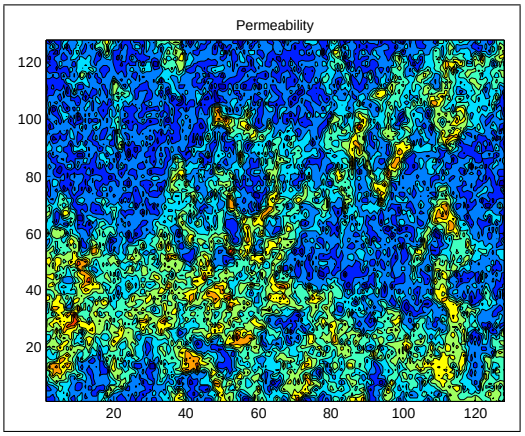

(a) x_k

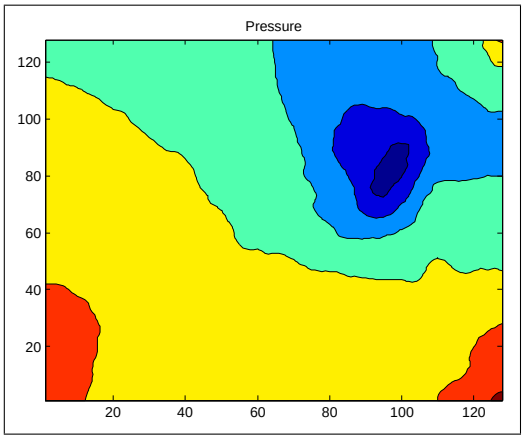

(b) $M(x_k)$

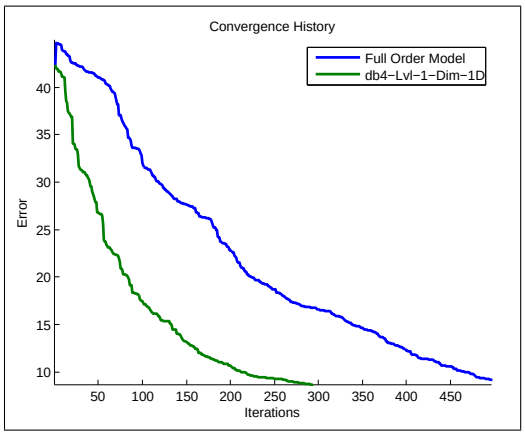

(c) Convergence History Comparison

Figure A.1: 4th Order Daubechies Decomposition Level 1 (1D)

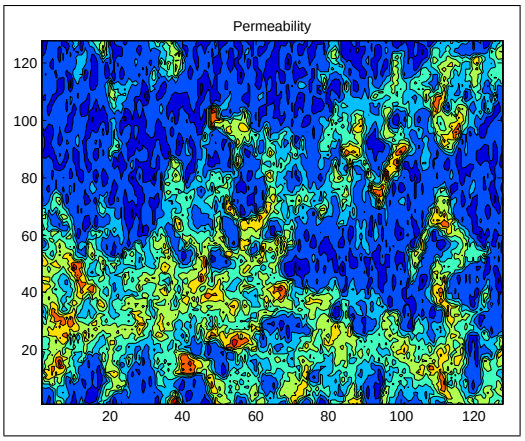

(a) x_k

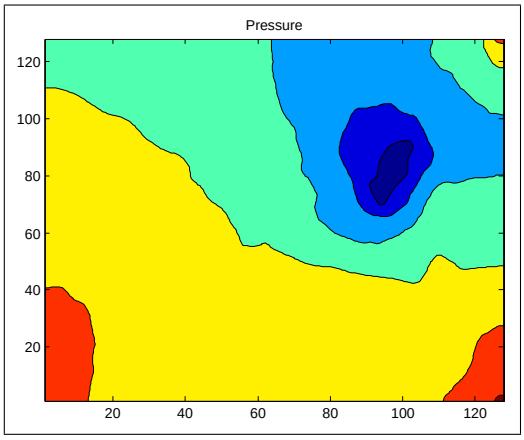

(b) $M(x_k)$

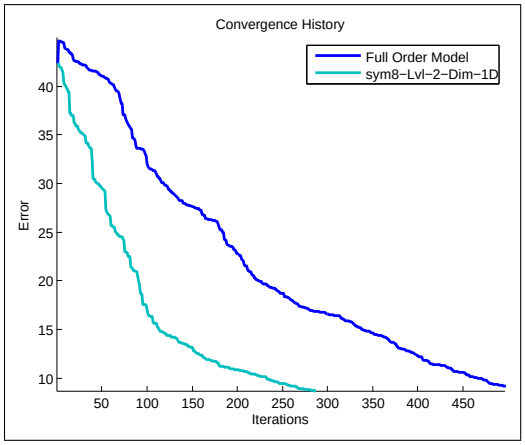

(c) Convergence History Comparison

Figure A.2: 8th Order Symlet Decomposition Level 2 (1D)

A.2 2D Permeability, Pressure and Convergence

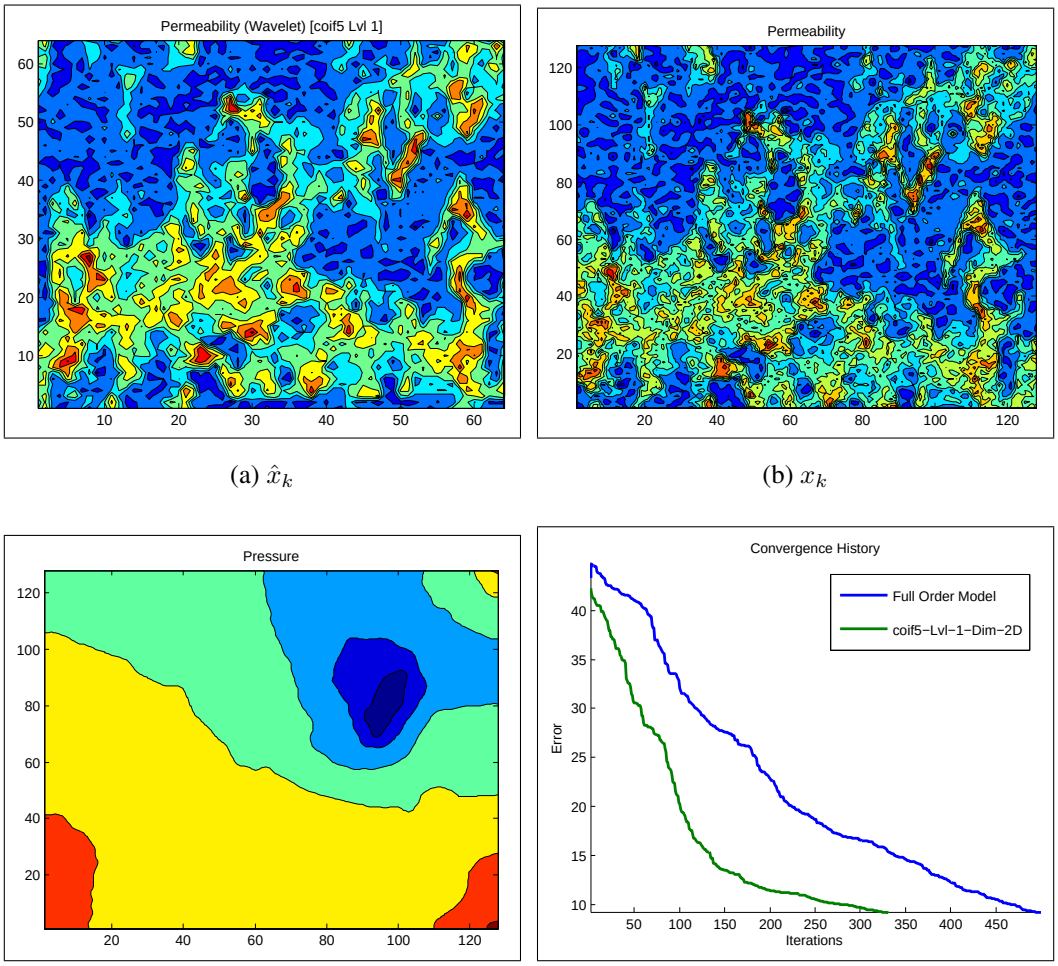

(a) $\hat{x}_k$

(b) x_k

(c) $M(x_k)$

(d) Convergence History Comparison

Figure A.3: 5th Order Coiflet Decomposition Level 1 (2D)

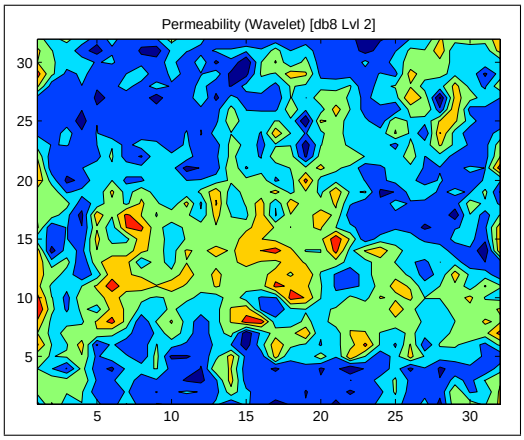

(a) $\hat{x}_k$

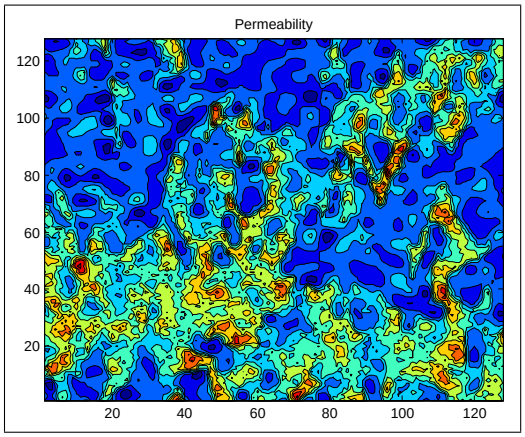

(b) x_k

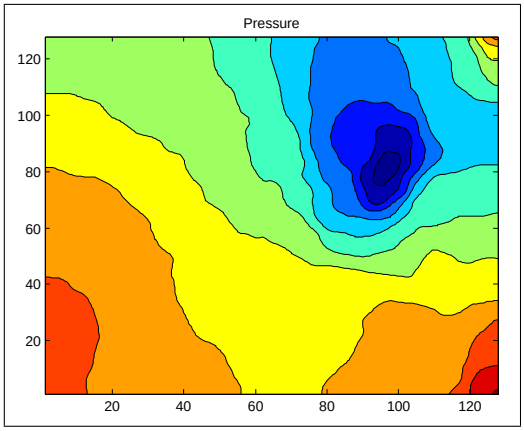

(c) $M(x_k)$

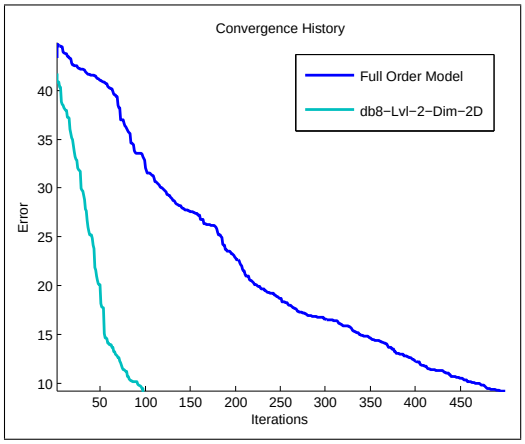

(d) Convergence History Comparison

Figure A.4: 8th Order Daubechies Decomposition Level 2 (2D)

Curriculum Vitae

Miguel Hernandez IV graduated third in his class in 1998 from Parkland High School and began studies at The University of Texas at El Paso as a Presidential Scholar. In 1999, Miguel was awarded The National Action Council for Minorities in Engineering (NACME) Corporate Scholarship. In 2000 and 2002, he became a member of Eta Kappa Nu and Tau Beta Pi respectively. During the summers of 2001 - 2003, he interned at Texas Instruments in Houston, Texas. Miguel received a Bachelor of Science in Electrical Engineering with Highest Honors (Summa Cum Laude) in May 2003. In the Fall of 2003, he entered the Graduate School at The University of Texas at El Paso as a fellow of the National Consortium for Graduate Degrees for Minorities in Engineering and Science (GEM) and the National Science Foundation (NSF). During the summer of 2004, he interned one last time with Texas Instruments. In May 2005, Miguel received a Master of Science in Electrical Engineering and began employment with the U.S. Army Research Laboratory as an Electronics Engineer. During the Fall of 2009, he returned to the University of Texas at El Paso to begin graduate studies in Computational Science. In December 2011, Miguel received a Master of Science in Computational Science.